Ocean-recharge oscillator model of the El Nino Southern Oscillation (ENSO)

Matthew Goodwin, University of Reading

This project aims to reproduce a model of the oscillation of Eastern Pacific Sea surface temperature anomaly (T) and West Pacific ocean thermocline depth (h), based on that of Jin 1997. Using this model the effects of non-linearity and forcing on coupled systems will be investigated.

The ENSO oscillation originates in interactions between the ocean and atmosphere.

Coupling between surface wind stress and thermocline depth is the essential mechanism that creates the oscillation.

Bjerknes positive feedback – The default state of Sea surface temperature (SST) in the East Pacific is colder than expected, and likewise the West is anomalously warm- therefore a gradient in SST exists along the Pacific.

In the atmosphere, over the West Pacific, warmer temperatures cause air near the surface to become more convective, and in the cool East, air subsidence increases- the atmospheric circulation increasing in strength leads to stronger trade winds blowing from East to West along the equator.

During this La Nina state, as a result of the trade winds blowing more strongly, transport of warm water to the West Pacific is increased, drawing up deeper, colder water in the Eastern Pacific, reducing thermocline depth (the barrier bewteen warm and cold water). This reinforces the SST anomalies, a positive feedback loop! Analogously a similar feedback mechanism exists to reinforce the El Nino state.

As a result, if this was the only process, ENSO would stay in either El Nino or La Nina state and not change from one to the other. Another process is therefore required to change the ENSO state.

Jin 1997 proposed a Recharge Oscillator Model (ROM), that brings to end the cold phase of East Pacific SST by recharge of zonal average ocean heat content as easterly wind stress drives

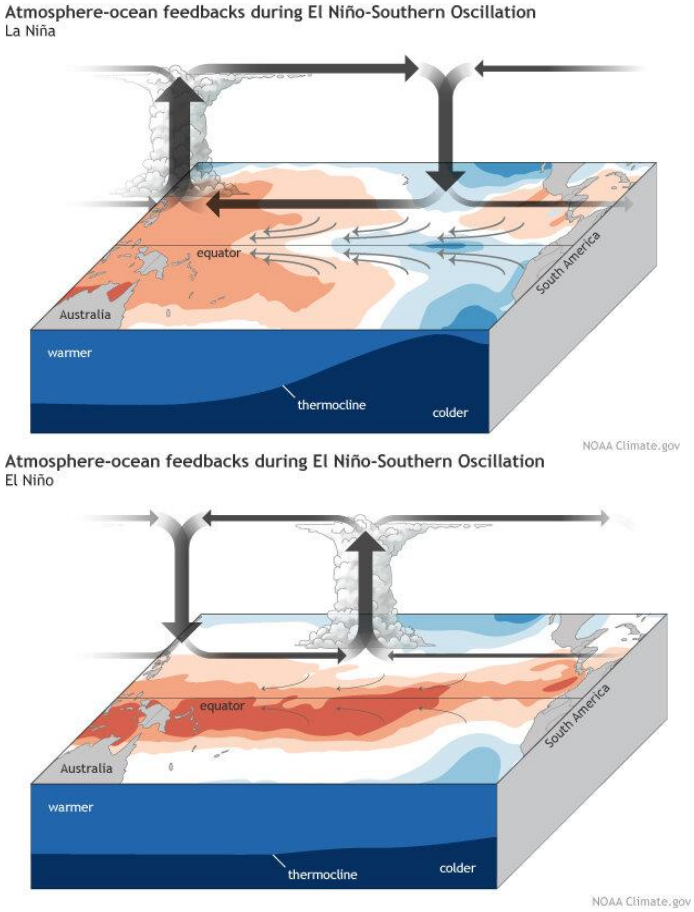

Figure 1: ENSO Bjerknes positive feedback mechanisms demonstrated for both El Nino and La Nina state

convergence of Sverdrup transport in the ocean. Jin describes this Recharge Oscillator model with two ODEs (Ordinary differential equations):

$$\frac{dh_w}{dt} = -rh_w - \alpha bT_E - \alpha\xi_1$$

$$\frac{dT_E}{dt} = RT_E + \gamma h_w - e_n(h_w + bT_E)^3 + \gamma\xi_1 + \xi_2$$

Where T_E is the East Pacific SST anomaly, h_w the West Pacific ocean thermocline depth, and t time.

Parameters:

b is a measure of thermocline slope, $b = b_0\mu$, where μ is the coupling coefficent and b_0 is the high end value of the coupling parameter, set to 2.5.

γ is the feedback of the thermocline gradient on the SST gradient, set to 0.75

c is the damping rate of SST anomalies, set to c = 1

R = γb – c, describing the Bjerknes positive feedback process.

r = 0.25, representing damping of upper ocean heat content

α = 0.125, relating enchanced easterly wind stress to the recharge of ocean heat content

e_n allows the degree of non linearity of the system to be varied, initially set to zero.

The random wind stress forcing is given by ξ_1

The model is also non-dimensionalised using:

SST temperature anomaly scale = 7.5K

Thermocline depth scale = 150m

Timescale = 2 months

Numerical implementation:

In order to solve these coupled equations numerically, a Huen scheme is used.

The Matsuno and Huen time schemes are examples of Iterative time schemes, also known as predictor-corrector schemes. In a two-step iterative scheme, the first step is the predictor, and the second the corrector, which allows higher accuracy with longer time-steps compared to non-iterative schemes, but as the cost of having to evaluate the function several times, which could be computationally expensive.

$$\frac{q^{n+1} - q^n}{\Delta t} = \beta^* f^{n+1^*} + \alpha f^n$$

Where q^{n+1^*} is a provisional value for q^{n+1}, calculated using the Euler method, and this is used to calculate f^{n+1^*}

$$\frac{q^{n+1^*} - q^n}{\Delta t} = f^n$$

When β* = 1 and α = 0, this reduces to the Matsuno scheme, whereas the Huen scheme uses β* = ½ and α = ½ . The Matsuno scheme imitates the backwards scheme, and the Huen scheme imitates the trapezoidal scheme, but it is important to note than neither are actually implicit schemes, as they do not require knowledge of past timesteps. Matsuno is first order accurate, whereas Huen is second order accurate, demonstrating the ability for iteration to improve the order of accuracy.

The Huen scheme can be thought of graphically as attempting to adjust a tangent to the curve in time.

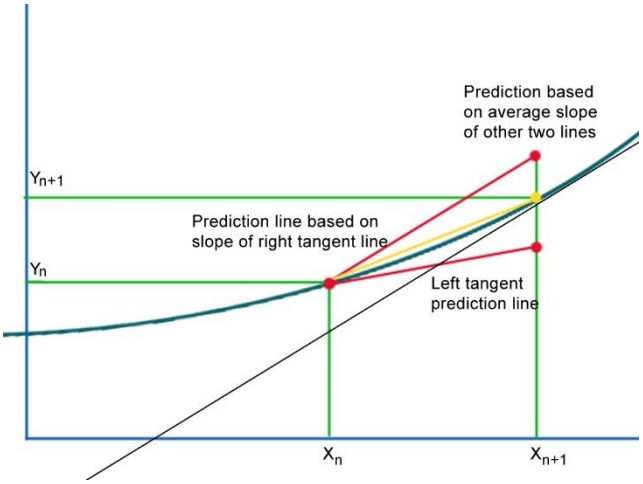

Figure 2: Graphical depiction of Huen numerical scheme for solving ODE (Wikipedia commons)

Euler's method uses a line tangent to function at the start of the interval to estimate the gradient over the whole interval, which has a small error if the timestep is small. However, even with small timesteps this error will accumulate after a large total number of timesteps. The Huen method uses tangents (calculated by the Euler method) to the curve at both ends of the timestep; one of the tangents will overestimate the gradient, and the other will underestimate. An average of the two will therefore give approximately halfway between the overestimation and underestimation, and a more accurate estimation of the true gradient (and therefore true value at next timestep).

Implementation:

Two functions have been used to calculate dh/dt and dT/dt, given inputs for T and h. These functions are f and g.

Another function is then defined, ENSO_Matsuno_Huen, which implements either Matsuno or Huen depending on the value of beta* (by default set to beta = 0.5, which is the Huen method).

$$h_{new} = h + \Delta t(\beta^* \times f(h^*, T^*) + (1 - \beta^*) \times f(h, T))$$

Then the function main calls this function twice, the first time to calculate the values of h* and T*. This is done by passing in h^n and T^n (values at current timestep)

for both h, T and h* and T* into the ENSO_Matsuno_Huen function, which now simplifies to:

$$h^* = h + \Delta t(\beta^* \times f(h, T) + (1-\beta^*) \times f(h, T))$$

And for β* = 0.5, simplifies down to the Euler scheme,

$$h^* = h + \Delta t \times f(h, T)$$

Now the ENSO_Matsuno_Huen function is called again, this time with h^n, T^n, h* and T*, which adjusts the prediction to a new value, which is taken as h^{n+1} and T^{n+1}

$$h^{n+1} = h^n + \Delta t(\beta^* \times f(h^*, T^*) + (1-\beta^*) \times f(h^n, T^n))$$

$$T^{n+1} = T^n + \Delta t(\beta^* \times g(h^*, T^*) + (1-\beta^*) \times g(h^n, T^n))$$

This process repeats for the required number of timesteps.

Von Neumann Stability analysis:

In order to derive the stability of the Huen scheme mathematically, the Amplification factor (A) must be evaluated from the system of equations, written in matrix form. For Huen, this leads to $A = B^{-1} C$, where

$B = I - \Delta t \begin{pmatrix} -r & -\alpha\beta \\ \gamma & r \end{pmatrix}$ and,

$C = I + \frac{1}{2}\begin{pmatrix} -r & -\alpha\beta \\ \gamma & r \end{pmatrix}$,

Which, using Python github library to calculate eigenvalues and substitute for a very small (idealised) Δt, gives a final value for the magnitude of A = 1. This means the solutions will not grow unstable, or dampen, unlike with the Euler or Matsuno schemes.

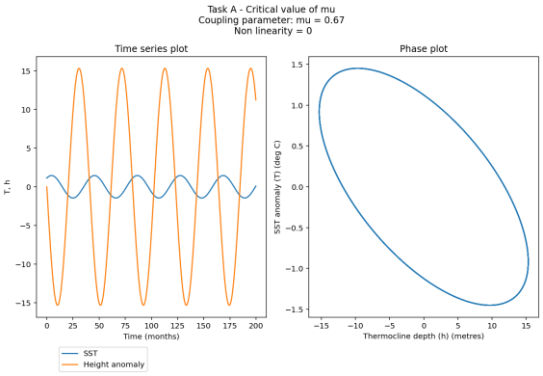

Figure 5: TASK A: Huen implementation of ENSO

TASK A: Neutral linear Recharge Oscillator

First the recharge oscillator is implemented without external forcing or non-linearity, using the Huen numerical scheme.

The coupling parameter (μ) is initially set to its critical value = 2/3, which was shown by Jin(1997) to produce a stable oscillation with frequency ω = $\sqrt{3/32}$, and therefore time period = 2π/ ω = 41 months when dimensionalised.

It is easy to see graphically from the phase plot of h and T that the Huen scheme is stable- whilst the model is run for several time periods, it continues to follow the same path around the ellipse of possible T, h values. In contrast, when Euler or Matsuno is used, the path is unstable, with T and h values gradually increasing in a spiral out from the original solutions, which matches the predicted amplification factor of greater than one from the Von-Neumann Stability analysis.

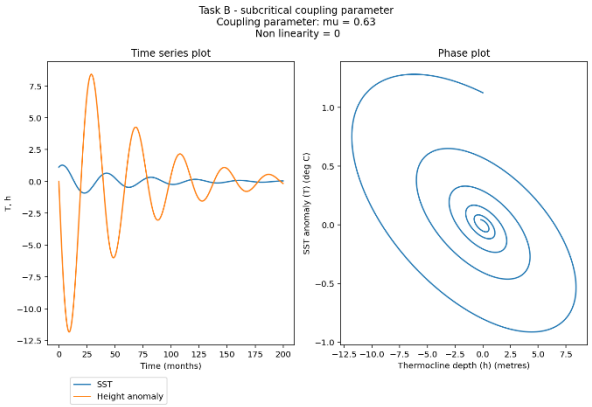

Figure 3: Subcritical case for μ, showing decaying solution (From TASK B)

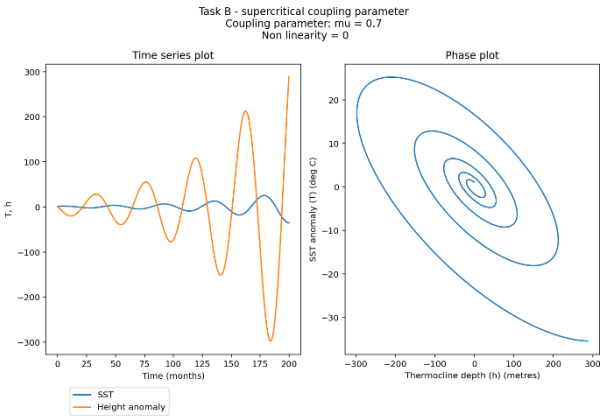

Figure 4: Supercritical case for μ, showing unstable solution (From TASK B)

TASK B: Recharge oscillator behaviour around the critical coupling parameter

The model is re-run for approximately 5 time periods (corresponding to 1000 timesteps, with the timestep size = 0.1), once for a subcritical value of coupling parameter (μ = 0.63) and then for supercritical value (μ = 0.75). For the subcritical value, in phase space the trajectory curls in an inward spiral, as the values of h and T decrease due to the damped oscillator. For the supercritical value, the trajectory instead curls in an outward spiral, as the values of h and T increase exponentially due to the unstable oscillator. Increasing the value of μ above the critical value increases the rate of instability growth, and similarly, decreasing the value of μ below the critical value increases the rate of oscillation damping. This can be seen also in the time series plots for both cases, with the amplitude of the oscillations increasing for the supercritical case and decreasing for the subcritical case.

TASK C: Extending Recharge Oscillator to include impact of non-linearity

Non-linearity is turned on by setting e_n = 0.1, and the model is run again at the previous critical value of the coupling parameter (μ = 2/3). The figure below shows a comparison between the non-linear case and the linear case. This is then repeated for increasing values of the coupling parameter.

Increasing μ to supercritical values in the linear case ($\mu > 2/3$) causes the phase plot to become increasingly unstable, and the time series plots for T and h to have increasing amplitude oscillations. However, for the *non-linear* case the solution initially grows in amplitude, but this growth levels off to a maximum amplitude stable oscillation. Further increasing μ in turn leads to a larger final value for both T and h (although the increase in final value for SST is much smaller than the increase in final value for h), but the oscillation still reaches stability.

This is confirmed by the phase plot, which initially grows, curling outwards similar to the linear case, but then reaches a stable solution, and continues to cycle around this. Higher μ values also lead to less cycles before the oscillation reaches its maxima.

Importantly, the critical value for μ has now changed (*increased*)- this is illustrated by $\mu = 0.67$ (Figure 6) and $\mu = 0.68$ (Figure 7) plots, as for $\mu = 0.67$ the solution is clearly damping (seen as decreasing amplitude on the time series plot, and spiralling inwards for the phase plot), whereas for $\mu = 0.68$, the solution reaches stable oscillations. This means the new critical value is between these two values and was found to be around $\mu = 0.672$.

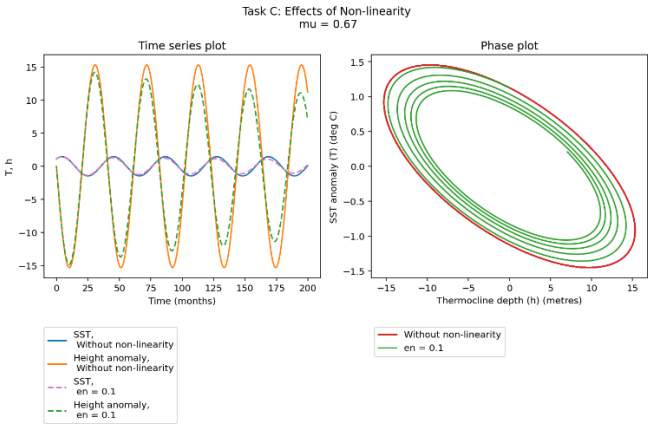

Figure 6: TASK C: Effects of non-linearity, with solution before and after non-linearity introduced displayed, μ = 2/3 (Critical value). Clear decaying of solution seen in non-linear case (green)

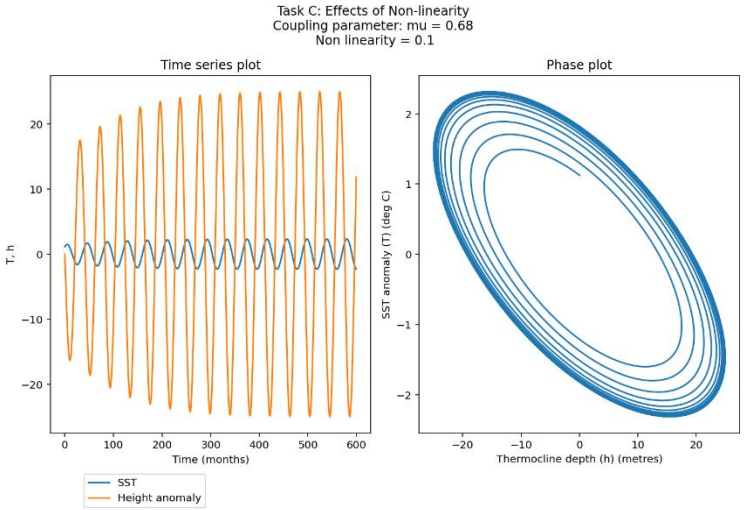

Figure 7: Non-linear solution for higher μ value- whereas previously this μ value would be unstable, the solution now reaches a peak and stability

Task D: Self-excitation hypothesis:

Annual frequency is introduced by allowing μ (coupling parameter) to vary on an annual cycle using:

$$\mu = \mu_0(1 + \mu_{ann}\cos(\frac{2\pi t}{\tau} - \frac{5\pi}{6})$$

Non-linearity parameter is kept at e_n = 0.1, the initial coupling parameter value μ_0 = 0.75, μ_{ann} = 0.2, and τ = 12 months (representing the annual cycle). In order for tau units to be consistent with t, tau is set to τ = 24 / (t_scale). t (current time) to be kept consistent with units of months is set a n * dt * t_scale, where n is the current timestep.

Both b (thermocline slope) and R (Bjerknes positive feedback) must be updated each timestep due to their dependency on the now varying value of μ. A graph of μ with time showing how μ varies with a time period of 12 months can be seen in the appendix.

On the time series plot, it can be seen how each peak is similar to the original without varying coupling parameter, except with slightly varying frequency and amplitude. Although the coupling parameter varies annually, the effects on the long-term ENSO cycle (period 41 months) are apparent, with some years having a larger height and SST than expected, and some smaller, without a clear periodic pattern.

The phase plot displays 'wavy' behaviour, as although the solution has still converged to roughly the ellipse of the original, the variation in coupling parameter causes large deviations from this.

Task E: Stochastic initiation hypothesis

Now a crude physical parameterisation is added for wind stress forcing. This term, ξ_1, is modelled using the equation below:

$$\xi_1 = f_{ann}\cos\frac{2\pi t}{\tau} + f_{ran}W\frac{\tau_{cor}}{\Delta t}$$

This has an annual cycle component, and a random daily component. The weighting of each of these components is given by f_{ann} = 0.02 and f_{ran} = 0.2, which means the random component has 10 times greater weighting than the annual cycle. The randomness is generated by W, which is a random number between 0 and 1 (different with each time-step).

The stochasticity is evident on the phase plot as noise on the curve. At higher values for μ_0, the model goes unstable, and the stochasticity is small in comparison so cannot be seen on the phase plot.

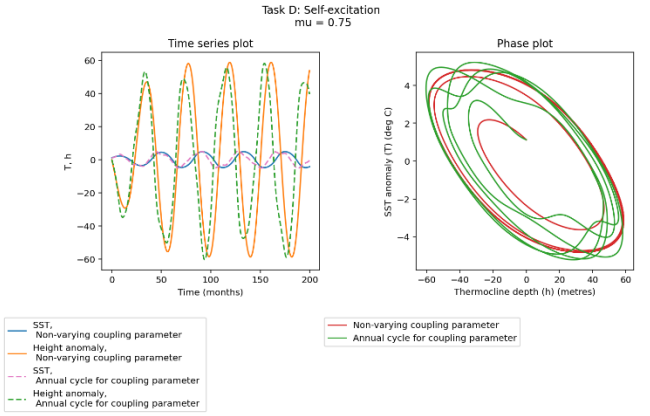

Figure 8: Introduction of annual cycle to μ, non-linearity included.

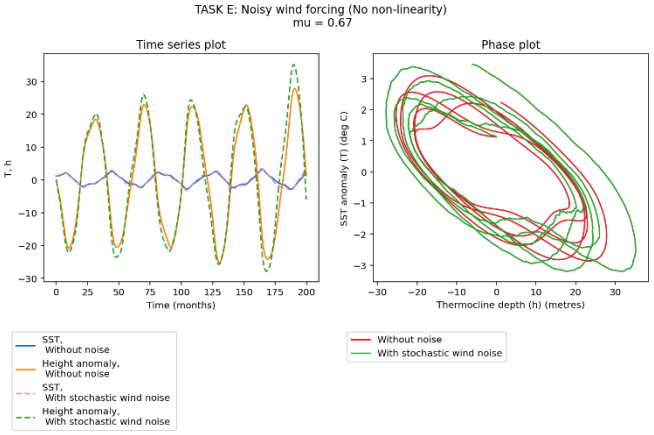

Figure 9: Wind stress parameterisation added to linear model.

Task F: Stochastic wind forcing + Non linearity together

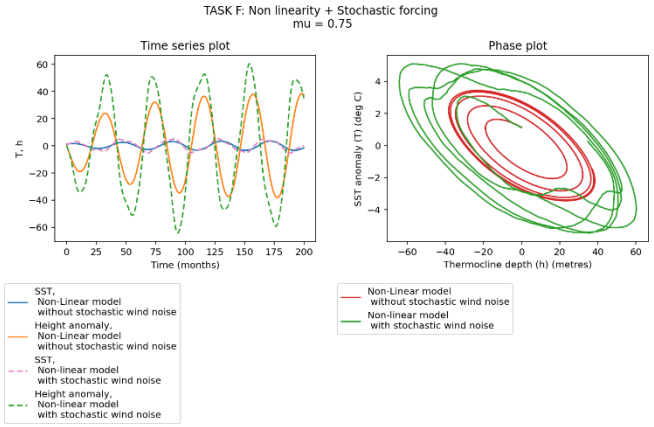

Figure 10: Non-linear model with stochastic wind-forcing

Testing both non-linearity and the stochastic wind forcing together, shows a stable solution, compared to the linear case with wind forcing, with the same value for μ, which is unstable. The wind forcing had led to a much larger value solution for h and T, but still stable. The irregular nature of the solution indicates the *possibility* of chaos.

Task G: Ensemble experiment

The irregular nature of the forecast trajectories indicates that the model may be sensitive to initial conditions, which could imply chaotic behaviour. A forecast ensemble is used assess the spread of ENSO forecasts to a) Uncertainty in initial conditions for h_w and T_E, b) Random wind stress forcing and c) both cases at the same time. Figure 11 displays condition c, and cases a and b can be seen in the Appendix.

Conclusion – does the Jin model reproduce chaotic behaviour?

Chaos is aperiodic behaviour in a deterministic system with sensitive dependence on the initial conditions. However, it can be seen from the Ensemble experiment, that although different initial conditions lead to different forecasts for SST and thermocline depth, the resulting pattern is periodic, and the forecast solutions do not diverge from each other chaotically – after long enough the system has 'forgotten' the initial conditions.

This is demonstrated by increasing the spread of the random initial conditions, to very large values. This does not increase the spread of the resulting forecast as the solution still converges onto the same attractor, visible in the phase plot Figure 12.

The Poincare Bendixson theorem states that for a system to exhibit chaotic behaviour, it must be three dimensional (unless time dependent forcing is added). As such, this simple system will not behave chaotically and instead needs a third coupled equation to be included.

Vallis 1986 describes a successful chaotic model of ENSO. The resultant oscillation is a strange attractor, with the one oscillation solution representing normal feedback, and the rarer 'wing' the El Nino state. (Figure 13) In Vallis 1986, three variables are used, SST in the West and East, and a wind driven current advecting the temperature field. Vallis's model is naturally chaotic, and aperiodically produces El Nino events. Also no stochastic or seasonal varying forcing is used. El Nino states are orbits around another, more unstable solution, so the

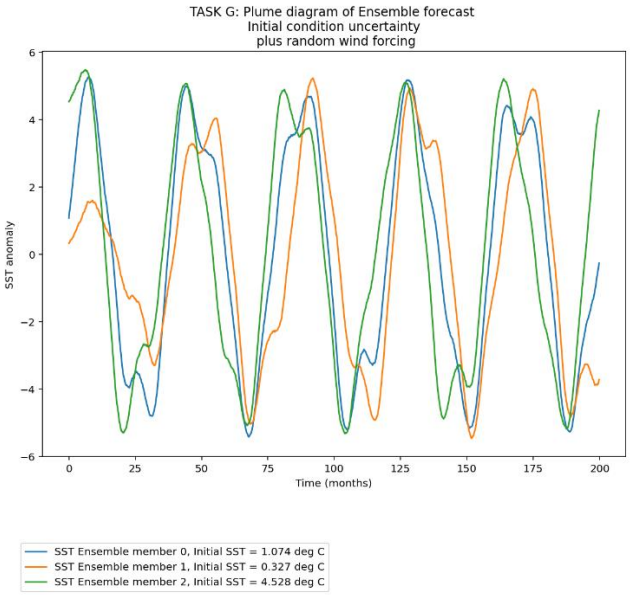

Figure 11: Ensemble forecast for SST using varying initial conditions for both SST and thermocline height

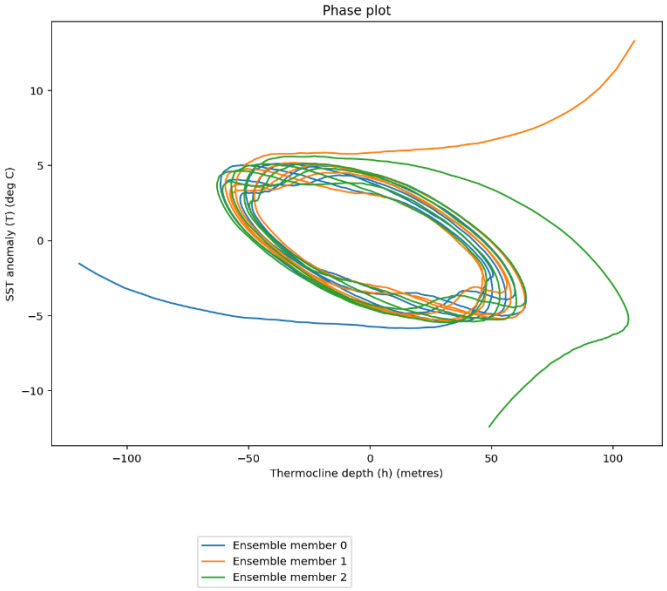

Figure 12: Phase plot showing three wildly varying different initial conditions. It is clear from the plot that all three ensemble members quickly converge to the same attractor

system quickly returns to a normal, more stable state.
An annual cycle of the trade winds shows that El Nino events are partially phase-locked to this annual cycle, as the system can only break into an El Nino state when the trade winds are weak (which is realistic of observed ENSO behaviour). Vallis also suggests that it may be possible to produce chaotic behaviour with a two-variable model, with SST difference and seasonal forcing of the trade winds.

Therefore, to add chaotic behaviour into the Jin model, a third equation linking the trade winds with SST would be needed.

References:

El Nino: A Chaotic Dynamical System?, Vallis, 1986
An Equatorial Ocean Recharge Paradigm for ENSO: Jin, 1996

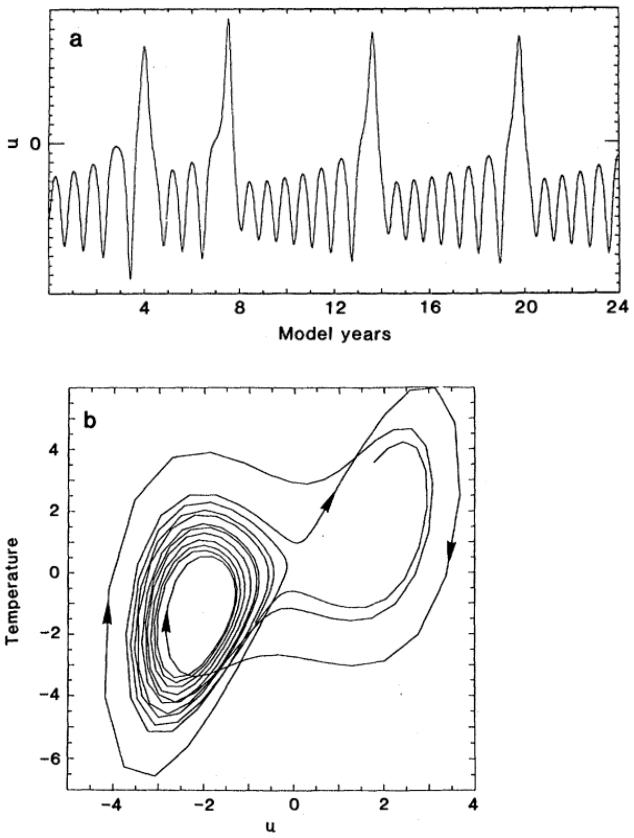

Figure 13:Taken from Vallis 1986, showing their model producing El Nino events, seen as the rare high temp and high u 'wing' of the phase plot, and as aperiodic spikes on the time series profile.

Appendix:

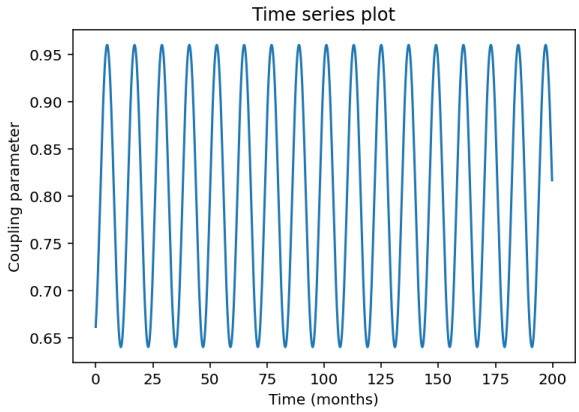

Figure 14: Annual cycle for coupling parameter (μ)

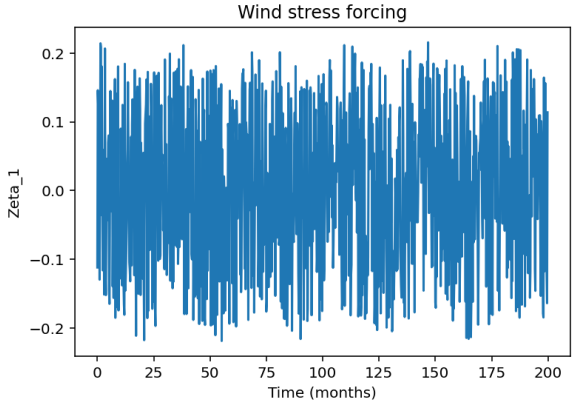

Figure 15: Variation in wind stress forcing parameter ξ_1

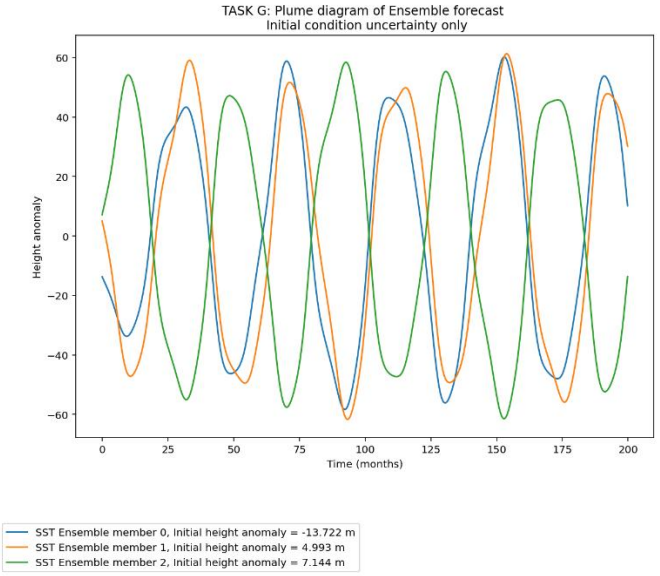

Figure 16: Ensemble forecast with just initial condition perturbations, no random wind forcing

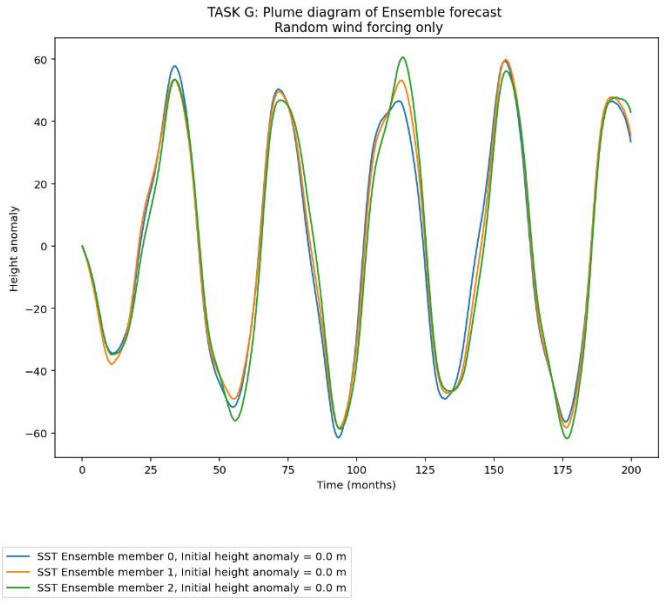

Figure 17: Ensemble forecast, with random wind forcing, and no variation in initial conditions